

## Surface and contact forces models within the framework of microassembly

PIERRE LAMBERT<sup>1</sup> and STÉPHANE RÉGNIER<sup>2,\*</sup>

<sup>1</sup>*BEAMS Department (CP165/14), ULB – 50, Av. F.D. Roosevelt, B-1050 Brussels, Belgium*

<sup>2</sup>*Laboratoire de Robotique de Paris, Université Pierre et Marie Curie (Paris VI), CNRS-FRE 2507, 18 Route du Panorama, F-92265, Fontenay Aux Roses, France*

**Abstract**—This paper gives a review of existing models used by other authors aiming at modeling micromanipulation tasks. It introduces the distinction between surface forces, which act even at distance (van der Waals (VDW), capillary and electrostatic forces) and contact forces, which are closely related to deformation and adhesion. Moreover, it presents our work on VDW and capillary forces: compared to existing approximations, these models allow to take more parameters into account such as, for example, statistical roughness in VDW forces or the volume of liquid in capillary forces. They could be used, for example, to build up new handling strategies as illustrated in the references cited in the paper. However, this paper focuses on fundamental models and does not present any specific microhandling strategy.

**Keywords:** Micromanipulation; adhesion forces; microassembly; microgripping; surface forces; contact forces; deformation.

### NOMENCLATURE

|                     |   |                                 |
|---------------------|---|---------------------------------|
| $A$                 | Hamaker constant  | J                               |
| $A_{ikj}$           | Hamaker constant (media $i$ and $j$ separated by a medium $k$ ) | J                               |
| $B_0$               | Bond number   | (dimensionless)                 |
| $C$                 | van der Waals interaction constant (all contributions)          | $\text{J m}^6 \text{ mol}^{-2}$ |
| $C_R$               | Retardation effects constant                                    | $\text{J m}^7 \text{ mol}^{-2}$ |
| $C_a$               | Capillary number  | (dimensionless)                 |
| $C_{\text{ind}}$    | Induction interaction constant                                  | $\text{J m}^6 \text{ mol}^{-2}$ |
| $C_{\text{orient}}$ | Orientation interaction constant                                | $\text{J m}^6 \text{ mol}^{-2}$ |

---

\*To whom correspondence should be addressed. E-mail: [regnier@robot.jussieu.fr](mailto:regnier@robot.jussieu.fr)

|                   |  |   |
|-------------------|--|---|
| $C_{\text{disp}}$ | Dispersion interaction constant                                | $\text{J m}^6 \text{mol}^{-2}$                          |
| $C_0$             | Electrical capacity of two conductive solids                   | F   |
| $d$               | Separation distance between a molecule and a solid             | m   |
| $e$               | Electron charge  | $(1.602 \times 10^{-19} \text{ C})$                     |
| $E$               | Young modulus  | GPa   |
|                   | Electric field   | $\text{V m}^{-1}$                                       |
| $E_A, E_D$        | Energy level   | eV  |
| $F_{\text{VDW}}$  | van der Waals force  | N   |
| $F_L$             | Laplace term of the capillary force                            | N   |
| $F_T$             | Interfacial tension term of the capillary force                | N   |
| $g$               | Earth gravity  | $9.81 \text{ ms}^{-2}$                                  |
| $h$               | Planck constant  | $(6.626 \times 10^{-34} \text{ m}^2 \text{ kg s}^{-1})$ |
|                   | Immersion height   | m   |
| $H$               | Mean curvature of the meniscus surface                         | $\text{m}^{-1}$   |
| $H_{\text{LV}}$   | Lifshitz–van der Waals constant                                | J   |
| JKR               | Refers to Johnson-Kendall-Roberts model                        | (dimensionless)   |
| $k$               | Boltzmann constant   | $(1.381 \times 10^{-23} \text{ J K}^{-1})$              |
| $L$               | Width of the rectangular box (VDW)                             | m   |
| $L_C$             | Capillary length   | m   |
| $m$               | Electron mass  | kg  |
| $n$               | refractive index   | (dimensionless)   |
| $n_A$             | density of states  |   |
| $n_1, n_2$        | density of ions  |   |
| $N_E$             | density of traps   |   |
| $p_{\text{in}}$   | Pressure in the liquid phase                                   | Pa  |
| $p_{\text{out}}$  | Pressure in the vapor phase                                    | Pa  |
| $q$               | Electrical charge  | C   |
| $r$               | Distance between two molecules                                 | m   |
| $r(z)$            | Equation of the meniscus profile in the axially symmetric case | m   |
| $r_1$             | Radius of the liquid bridge at the component side              | m   |
| $r_2$             | Radius of the liquid bridge at the gripper side                | m   |
| $r_k$             | Depth of the $k$ th cut in the discretized roughness profile   | m   |
| $R$               | Sphere radius (VDW)  | m   |
|                   | Radius of a droplet posed on the substrate                     | m   |
|                   | Radius of spherical grippers                                   | m   |
|                   | Molar gas constant   | $(8.314 \text{ J K}^{-1} \text{ mol}^{-1})$             |
| $R_a$             | Roughness parameter (arithmetic mean)                          | m   |

|                  |  |                                  |
|------------------|--|----------------------------------|
| $S$              | Area of the rectangular box section parallel to the half-space           | m                                |
|                  | Lateral area of the meniscus (i.e. area of the L-V interface)            | m <sup>2</sup>                   |
| $S_k$            | Area of the $k$ th cut of the discretized roughness profile              | m                                |
| $T$              | Absolute temperature   | K                                |
| $\Delta U$       | potential  | eV                               |
| $v$              | Molar volume   | m <sup>3</sup> mol <sup>-1</sup> |
| $V$              | Volume of liquid   | m <sup>3</sup>                   |
|                  | Electrical potential   | V                                |
| $V_C$            | Contact potential  | V                                |
| $w$              | van der Waals interaction potential between two dipoles (VDW)            | J mol <sup>-2</sup>              |
| $W$              | Component weight   | N                                |
|                  | VDW interaction potential between two macroscopic bodies                 | J                                |
|                  | Total interfacial energy of the meniscus (S-V, L-V, S-L)                 | J                                |
| $W_{LV}$         | Partial interfacial energy of the meniscus (L-V)                         | J                                |
| $W_{SL}$         | Partial interfacial energy of the meniscus (S-L)                         | J                                |
| $W_{SV}$         | Partial interfacial energy of the meniscus (S-V)                         | J                                |
| $W_{(S,HS)}$     | VDW interaction pot. between a sphere and an infinite half-space         | J                                |
| $W_{(p,p)}$      | VDW interaction potential between two infinite half-spaces               | J                                |
| $x$              | Usual coordinate   | m                                |
| $z$              | Separation distance between two solids                                   | m                                |
| <i>Greek</i>     |  |                                  |
| $\epsilon$       | Relative permittivity, dielectric constant                               | (dimensionless)                  |
| $\epsilon(i\nu)$ | Complex dielectric constant  |                                  |
| $\epsilon_0$     | Permittivity of free space ( $8.854 \times 10^{-12}$ F m <sup>-1</sup> ) | F m <sup>-1</sup>                |
| $\phi_1, \phi_2$ | Fermi levels   | eV                               |
| $\phi_1$         | Slope of the component at the location of the triple line                | rad                              |
| $\gamma$         | Surface tension of a liquid  | N m <sup>-1</sup>                |
|                  | Energy of the interface liquid-vapor                                     | J m <sup>-2</sup>                |
| $\gamma_{SL}$    | Energy of the interface solid-liquid                                     | J m <sup>-2</sup>                |
| $\gamma_{SV}$    | Energy of the interface solid-vapor                                      | J m <sup>-2</sup>                |
| $\nu$            | Frequency  | Hz                               |
| $\nu_e$          | Electronic frequency   | Hz                               |
| $\rho$           | Principal curvature radius of the liquid bridge (usually negative)       | m                                |
|                  | Density  | kg m <sup>-3</sup>               |
|                  | Molecular density  | mol m <sup>-3</sup>              |

|                  |  |                     |
|------------------|--|---------------------|
|                  | Volumetric charge density  | $\text{C m}^{-3}$   |
| $\rho_1(\rho_2)$ | Molecular density of material 1(2)                                 | $\text{mol m}^{-3}$ |
| $\rho'$          | Principal curvature radius of the liquid bridge (usually positive) | m                   |
| $\sigma$         | Superficial charge density   | $\text{C m}^{-1}$   |
| $\theta_1$       | Contact angle at the component side                                | rad                 |
| $\theta_2$       | Contact angle at the gripper side                                  | rad                 |
| $\xi$            | Coordinate of a volume element                                     | m                   |

## 1. INTRODUCTION

This paper is a review of microassembly, which can be defined as the assembly (i.e., sorting, feeding, picking up, positioning, controlling, releasing and joining) of microcomponents. Figure 1 indicates the scales and sizes discussed in this paper: boundaries are defined with information from both models and literature. Compared to the macroscopic domain, which is assumed to be ruled by gravity effects, the micrometric domain is limited by an upper boundary (typically a few mm, i.e., the cut-off length of the capillary effects (namely the capillary length  $L_C = \sqrt{\gamma/\rho g}$ ; for water,  $L_C \approx 2.7$  mm)) and a lower boundary at about  $1 \mu\text{m}$ . The part of the micrometric domain between  $0.1$  and  $1$  mm has been defined in Ref. [1] as the mesoscopic domain (mesodomain). The nanometric domain extends from a few nm up to the micron and is the ultimate domain of mechanical engineering. The boundary between the atomic domain and the nanometric domain can be set around the typical size of a molecule (around  $0.2\text{--}0.4$  nm). The term microcomponent (microobject) refers to a(n) component (object) ranging from  $10 \mu\text{m}$  to several mm.

In the area of microassembly and micromanipulation, the current academic researches mainly cover three fields.

The first field concerns the applications as, for example, the assembly of (micro-electro)mechanical components with a size ranging from  $10 \mu\text{m}$  to several mm, the handling and assembly of biological objects usually smaller than  $1 \mu\text{m}$ . Despite the apparently large extent of this field there are hardly any well-established benchmark applications for the micromanipulation of small mechanical components. One of the reasons is the lack of industrial mass products, maybe due to the difficulties inherent to the scale effects leading to new dominant effects, such as surface and contact forces (these problematics are addressed in Ref. [2]).

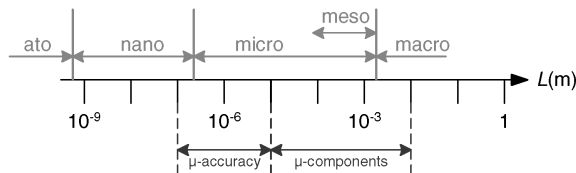


**Figure 1.** Sizes and scales referred to in this paper.

The second field covers the emerging technologies which have been extensively developed in the laboratories for a decade, most of them addressing the problematics of handling small components (typically small spheres with a diameter ranging from several  $\mu\text{m}$  to a few mm). These studies focused on the handling aspects of microassembly, i.e., essentially on the picking and releasing tasks. Many physical principles have been studied and, due to the disturbing effects of surface and contact forces, a lot of handling strategies have been proposed: these approaches can be structured in 4 groups according to the way they tackle the surface and contact forces [3]. These forces can be reduced, overcome or exploited as a gripping principle. Finally, a fourth strategy consists in avoiding contact by handling without contact. It is beyond the scope of this paper to review and sort out all these principles. More information on the subject can be found in Refs [3–7].

The third field of research is the less technological and the most physical one. It is also the less studied one. It consists of extracting elements data from the physical and chemical knowledge in order to build models, including the physics of the microscopic domain to describe the parameters and design rules of technological micromanipulation tools of the second field. Indeed, the theoretical models of the latter are quite limited although these approximations can be of the utmost interest in the case of simple geometries like spheres. They are unfortunately too limited to ensure the repeatability and reliability of more complex micromanipulation tasks. Modeling becomes even almost impossible for other tasks of microassembly such as, for example, joining by pressfit [8].

This paper is the result of research in this third field. It aims at covering the gap between existing knowledge in tribology on the one hand and the bad knowledge of design rules of microgrippers well adapted to the microscopic environment on the other hand. Therefore, here we focus on models which could be used to best design a micromanipulation task, without any consideration for the technological aspects. An extended example of this approach can be found in Ref. [3].

Before introducing the structure of this paper, let us briefly introduce some scaling law considerations. When downscaled, the volumetric forces (e.g., the gravity) tend to decrease faster than other kinds of forces, such as the capillary forces or the viscous force. Although these forces still exist at the macroscopic scale, they are often negligible (and neglected) in macroscopic assembly. A reduced system is consequently brought face to face with the relative increase of these so-called surface forces. As they decrease slower than the weight, there is always a cut-off size below which these forces disturb the handling task because they make the microcomponent stick to the tip of the gripper (the weight can no longer overcome them and ensure release). A classification of the forces as a function of their range is given Ref. [9] and presented in Table 1.

We propose to sort out these forces by making out whether there is contact or not. When there is no physical contact between two solids, the forces in action are called distance or surface forces (according to the scientific literature in this domain [4, 10, 11], these latter are electrostatic, van der Waals (VDW) and capillary

**Table 1.**  
Forces summary

| Interaction distance                  | Predominant force              |
|---------------------------------------|--------------------------------|
| Up to infinite range                  | Gravity                        |
| >From a few nm up to 1 mm             | Capillary forces               |
| > 0.3 nm                              | Coulomb (electrostatic) forces |
| 0.3 nm < separation distance < 100 nm | Lifshitz–van der Waals         |
| < 0.3 nm                              | Molecular interactions         |
| 0.1–0.2 nm                            | Chemical interactions          |

forces). When both solids contact each other, there are deformation and adhesion forces through the surfaces in contact. In this case, we consider contact forces and adhesion or pull-off forces. Electrostatic or capillary effects can be added, but VDW forces are not considered any longer, because they are already involved in the pull-off term.

Of course, it can be thought of additional forces like viscous drag or other effects related to the liquid environment like the electrostatic double layer effects. These aspects have been put aside here because we only consider a gaseous surrounding environment. More information about the forces acting in immersed microsystems can be found in Ref. [12].

The paper is structured as follows. First the problematics of surface forces (i.e., the forces which are also in action at a distance, when the component is not deformed by the contact forces) are presented in Section 2 and it is focused on VDW forces (Subsection 2.1), electrostatic forces (Subsection 2.2) and capillary forces (Subsection 2.3). Section 3 deals with contact forces and the related models and is focused on the interaction energy of two bodies (Subsection 3.2), deformations (Subsection 3.1) and friction (Subsection 3.4). Finally, the conclusion summarizes the contributions of this work and proposes tracks for further research.

## 2. SURFACE FORCES

### 2.1. Van der Waals forces

*2.1.1. Introduction.* The van der Waals (VDW) forces are often cited in papers dealing with micromanipulation and microassembly, probably because the founding papers of these bibliography reviews [10, 11] present these forces next to the capillary and the electrostatic forces as being of the utmost importance in the sticking of microparts. Other authors [13] prefer to neglect these forces because they are of a smaller order. The reasons for this opposition do not seem to be clear, all the more so since some authors propose to use adhesion as a suitable gripping principle [14, 15]. The will to clarify this situation was the first reason to study VDW forces. The second reason lies in the fact that most forces expressions used in the literature on microassembly are only approximations of simplified geometries

(spheres and planes). If these approximations are sufficient for experimental case studies, the influence of more complex geometries (non-symmetrical geometries), including roughness profiles, should be studied for microassembly applications. In this subsection, we summarize some analytical and numerical methods to compute these forces in non trivial geometries. An overview of the approximations from the literature is proposed in a conclusion of this subsection. For the reader who would be unfamiliar with these forces, a good and very didactic introduction to the subject can be found in Ref. [16].

For two dissimilar polar molecules interacting in the vacuum, the interaction potential is expressed as [17]:

$$w(r) = -\frac{[C_{\text{ind}} + C_{\text{orient}} + C_{\text{disp}}]}{r^6}, \quad (1)$$

where  $r$  represents the separation distance between the molecules and  $C_{\text{ind}}$ ,  $C_{\text{orient}}$  and  $C_{\text{disp}}$ , respectively, represent the contributions of the induction (Debye term), orientation (Keesom term) and dispersion (London term) phenomena to the interaction potential. This interaction potential between atoms is generally written as:

$$w(r) = -\frac{C}{r^6}. \quad (2)$$

The so-called retardation effect occurs when the separation distance increases over a cut-off length of the order of 5–10 nm. In this case, the decrease with the separation distance occurs faster and it is assumed that it can be described according to:

$$w(r) = -\frac{C_R}{r^7}. \quad (3)$$

The fast decrease of the VDW forces explains that they seem to be limited to the atomic domain. Nevertheless, this decrease occurs more slowly when we consider the interaction between two macroscopic bodies (that is, a body with a very large number of molecules, including bodies that have a size in the order of a few  $\mu\text{m}$  and that are consequently considered microcomponents when dealing with microassembly terminology). Therefore, it is not so obvious to determine whether these forces have to be dealt with or not.

There are two ways to compute the VDW interaction between two macroscopic bodies: the first one is known as the microscopic or Hamaker approach and the second one is called the macroscopic or Lifshitz approach.

From a strictly theoretical point of view, the VDW forces are non-additive, non-isotropic and retardated. However, in Ref. [18] a straight and powerful way to establish the potential interaction by assuming a pairwise additivity of the interactions has been proposed. Moreover, this approach does not consider the retardation effect. Therefore, the results are limited to separation distances between the retardation cut-off length (about 5–10 nm) and a lower separation distance equal to the equilibrium distance (about 0.1–0.2 nm) arising from the Lennard–Jones potential: for smaller separation distances, very strong repulsive forces occur

that can no longer be neglected. This lower limit is sometimes called the VDW radius [16]. We should bear in mind that, even with these restrictions, the results are not exactly correct for the interaction of solids and liquids because of the pairwise summation assumption. However, Refs [17] and [19] consider that these approximations are useful in several applications. We will illustrate this method in what follows.

The Lifshitz method, also called macroscopic approach, consists of considering as inducers of the two interacting objects as continuous media with a dielectric response to electromagnetic fields. The dispersion forces are then considered as inducers of the mutual interaction of dipoles oscillating at a given frequency. When the separation distance becomes larger than the cut-off length, depending on this frequency and the speed of light, the attraction tends to decrease because the propagation time becomes of the same order as the oscillation period of the dipoles, the field emitted by one dipole interacting with another dipole with a different phase. This effect has first been pointed out by Casimir and Polder [20] and computed by Lifshitz using the quantum field theory [21]. Although this approach is of the greatest complexity, similar results can be obtained by using Hamaker's results, on the condition to replace the Hamaker constant by a pseudo-constant involving more parameters. This method is out of our scope, which is to roughly evaluate the importance of the VDW forces in microassembly and to investigate the influence of geometry, roughness and orientation on the manipulation of microcomponents. We will, therefore, limit ourselves to the Hamaker method, despite its limitations. The interested reader will find further information about the Lifshitz approach in Ref. [22], chapter VI, and in Ref. [17]. The energy of interaction between a molecule and an infinite half-space (i.e., a body limited by a plane surface) will be the sum of the interactions between all molecules. It is assumed that the interaction between two molecules is not modified by the presence of neighbours (pairwise summation assumption).

*2.1.2. Analytical model: illustration of the Hamaker approach.* The Hamaker method is illustrated here below in the case of the interaction between a molecule, a sphere and a infinite half-plane on the one hand and another infinite half-space on the other hand. Figure 2 illustrates the mode of integration used in these cases.

If  $\rho$  is the molecular density of the infinite half-space (HS) and  $d$  the separation distance between the molecule and the surface, the interaction energy between this molecule and the HS is given by:

$$w(d) = -2\pi C\rho \int_{\xi=d}^{\xi=\infty} d\xi \int_{x=0}^{x=\infty} \frac{x dx}{(\xi^2 + x^2)^3} = -\frac{\pi C\rho}{2} \int_{\xi=d}^{\xi=\infty} \frac{d\xi}{\xi^4} = -\frac{\pi C\rho}{6d^3}, \quad (4)$$

where  $(\xi, x)$  are the coordinates of the volume element. We use several symbols for the separation distance:  $r$  denotes the separation distance between two molecules,  $d$  represents the distance between a molecule or a infinitesimal volume of molecules and a macroscopic body and  $z$  states for the separation distance between two

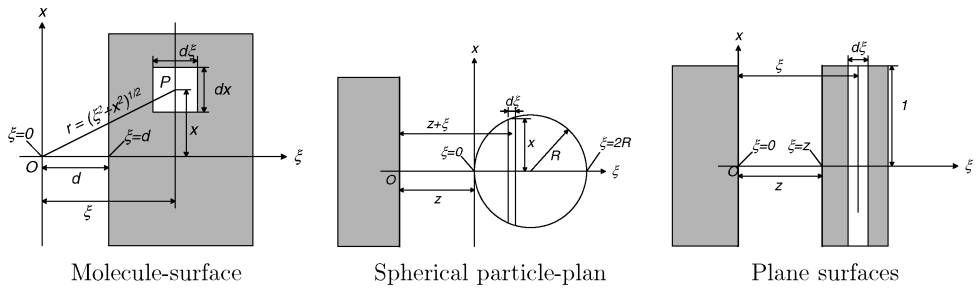


**Figure 2.** Integration mode.

macroscopic bodies. The interaction potential  $W_{(S,HS)}$  between a sphere and an infinite half-space can thus be calculated by adding the interactions of all the molecules of the sphere with the HS, assuming that the sphere is made of a material with the same molecular density  $\rho$ . By observing that the sphere can be cut into slices of radius  $x = \sqrt{R^2 - (\xi - R)^2}$  located at a distance  $z + \xi$  from the surface, the interaction potential  $W_{(S,HS)}$  between the HS and a sphere of radius  $R$  can be written as:

$$\begin{aligned}
 W_{(S,HS)}(z) &= -\frac{\pi^2 C \rho^2}{6} \int_{\xi=0}^{\xi=2R} \frac{(2R - \xi)\xi}{(z + \xi)^3} d\xi \\
 &= -\frac{\pi^2 C \rho^2}{6} \left[ \ln \frac{z}{2R + z} + \frac{2R(R + z)}{z(2R + z)} \right].
 \end{aligned}
 \tag{5}$$

For other surface geometries, the potential can be calculated a similar way. For example, the interaction potential by unit area between two parallel plates surfaces is given by:

$$W_{(p,p)}(z) = -\frac{\pi C \rho^2}{12z^2}.
 \tag{6}$$

By deriving the potential  $W$  with respect to the separation distance  $z$ , the van der Waals force  $F_{VDW}$  is given by:

$$F_{VDW}(z) = -\frac{dW(z)}{dz}.
 \tag{7}$$

A summary of the most frequent configurations is given in Table 2.

**2.1.3. Hamaker constant.** The quantity  $\pi^2 C \rho^2$  is rewritten into  $A$ , the Hamaker constant, which depends on the materials and the experimental conditions. It is generally obtained in experiments, but can also be calculated. Two theories exist on this subject.

1. According to Ref. [23] and in the case of dissimilar materials 1 and 2 characterized by different molecular densities  $\rho_1$  and  $\rho_2$ , the Hamaker constant is given by:

$$A_{12} = \pi^2 C \rho_1 \rho_2.
 \tag{8}$$

**Table 2.**Comparison of the approximations from the literature ( $z$ , separation distance;  $R$ , the sphere radius)

| Object 1 | Object 2         | Expression   | Reference                |
|----------|------------------|--|--------------------------|
| Plane    | Plane//          | $W = -\frac{A}{12\pi z^2}; F = \frac{A}{6\pi z^3}$<br>(by surface unit)  | [17, 22, 37]             |
| Cylinder | Cylinder //      | $W = -\frac{AL}{12\sqrt{2}z^{\frac{3}{2}}\left(\frac{R_1 R_2}{R_1 + R_2}\right)^{1/2}}; F = -\frac{3AL}{24\sqrt{2}z^{\frac{5}{2}}\left(\frac{R_1 R_2}{R_1 + R_2}\right)^{1/2}}$<br>( $L$ , cylinder length; $R_i$ , cylinder radius) | [17] and own results     |
| Cylinder | Cylinder $\perp$ | $W = -\frac{A\sqrt{R_1 R_2}}{6z}; F = \frac{A\sqrt{R_1 R_2}}{6z^2}$  | [17, 22] and own results |
| Sphere   | Plane            | $W = -\frac{AR}{6z}; F = \frac{AR}{6z^2}$  | [22, 37]                 |
| Sphere   | Sphere           | $W = -\frac{AR}{12z}; F = \frac{AR}{12z^2}$  | [17, 22, 37]             |

A usually takes values included in the interval  $(0.4-4) \times 10^{-19}$  J (values can be found in Ref. [9, 17, 22, 24]). This method provides good approximations of the constant for slightly polar materials, since it only takes the effect of dispersion into account and is obtained by assuming the additivity of the dispersion forces (pairwise summation assumption). In the opposite case, it underestimates its value.

2. Lifshitz [21] developed a more realistic theory which integrates the influence of the closer neighbouring atoms of considered pair. Therefore, the so-called retardation effect of the dispersion forces is less perceptible. The estimation of the Hamaker constant is however more complex. Indeed, it is necessary to know the variations of the complex dielectric constant ( $\epsilon$ ) of the materials involved in the system according to the frequency ( $\nu$ ). The Hamaker constant between two materials 1 and 2 separated by a medium 3 is given by [17]:

$$A_{132} \approx \frac{3}{4}kT \left( \frac{\epsilon_1 - \epsilon_3}{\epsilon_1 + \epsilon_3} \right) \left( \frac{\epsilon_2 - \epsilon_3}{\epsilon_2 + \epsilon_3} \right) + \frac{3h}{4\pi} \int_{\nu_1}^{\infty} \left( \frac{\epsilon_1(i\nu) - \epsilon_3(i\nu)}{\epsilon_1(i\nu) + \epsilon_3(i\nu)} \right) \left( \frac{\epsilon_2(i\nu) - \epsilon_3(i\nu)}{\epsilon_2(i\nu) + \epsilon_3(i\nu)} \right) d\nu. \quad (9)$$

Consequently, the Hamaker constant can be expressed by:

$$A_{132} \approx \frac{3}{4}kT \left( \frac{\epsilon_1 - \epsilon_3}{\epsilon_1 + \epsilon_3} \right) \left( \frac{\epsilon_2 - \epsilon_3}{\epsilon_2 + \epsilon_3} \right) + \frac{3h\nu_e}{8\sqrt{2}} \frac{(n_1^2 - n_3^2)(n_2^2 - n_3^2)}{\sqrt{(n_1^2 + n_3^2)}\sqrt{(n_2^2 + n_3^2)}[\sqrt{(n_1^2 + n_3^2)} + \sqrt{(n_2^2 + n_3^2)}]}, \quad (10)$$

where  $k$  is the Boltzmann constant ( $1.381 \times 10^{-23}$  J/K),  $T$  the temperature (K),  $\nu_e$  the principal electronic absorption frequency (typically about  $3 \times 10^{15}$  s $^{-1}$ ),  $\epsilon_i$  the dielectric constant and  $n_i$  the refraction index.

This complex expression can be simplified for more simple interactions (for example, for interactions 1–3–1, 1–2 or 1–1).

Sometimes it is possible to obtain approximated values of  $A$  by using so-called ‘combination laws’, derived from the expression of  $A$  introduced by MacLachlan in 1963 [25]: for two materials 1 and 2 interacting through vacuum,  $A_{12}$  is computed according to the constants  $A_{ii}$  of each material:

$$A_{12} \approx \sqrt{A_{11}A_{22}}.$$

In the same way, for two materials 1 and 2 interacting through a third one 3,  $A_{132}$  is approached by:

$$A_{132} \approx (\sqrt{A_{11}} - \sqrt{A_{33}})(\sqrt{A_{22}} - \sqrt{A_{33}}). \quad (11)$$

This combination law gives very good approximations of  $A$ , except in the case of strongly polar (high  $\epsilon$ ) media like water. In this case, the results of Equation (10) are closer to the experimental value. Reference [26] gives an expression for the VDW forces using the so-called Lifshitz–van der Waals constant, noted  $H_{LV}$  and expressed in eV (J). By this method, the VDW force between a sphere of radius  $R$  and an infinite half-space is expressed as [9]:

$$F_{\text{vdw}} = \frac{RH_{LV}}{8\pi z^2} \quad \text{and} \quad A = \frac{3H_{LV}}{4\pi} \text{ (J)}.$$

**2.1.4. Numerical formulation.** When geometries become non-obvious, summation cannot be achieved analytically. This subsection presents an example of numerical integration based on the Gauss integration method applied to the interaction between a sphere and another object (it could be for example a rectangular box) and a method based on the Green identity (also called the divergence theorem) used in order to study the influence of the relative orientation of the objects and that of their roughness.

**2.1.4.1. Gauss integration method.** In order to implement the Gauss method the integration domain must first be meshed with elementary cubes. Then, the function to integrate is evaluated at the mesh nodes and all these values are summed according to given weights [27]. The Gauss method guarantees that any defined integral can be calculated with:

$$\begin{aligned} \frac{1}{8h^3} \int \int \int_C f(x, y, z) \, dx \, dy \, dz = & \frac{1}{450} \left( -496 f_m + 128 \sum f_t + 8 \sum f_f \right. \\ & \left. + 5 \sum f_v \right) + O(h^6), \end{aligned} \quad (12)$$

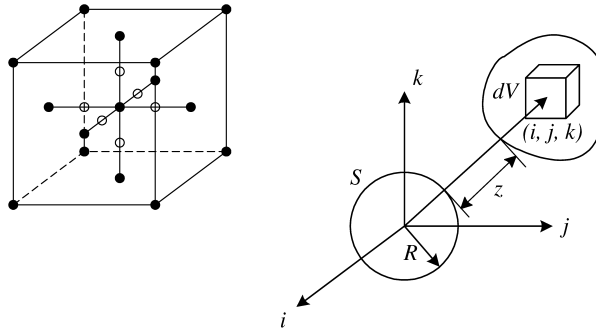


**Figure 3.** (left) Elementary cube in the Gauss method and its nodes. (right) Interaction between a sphere and any other shape.

where  $\sum f_r$  = sum of the values of  $f$  at the 6 midpoints of the segments linking the center of the cube to the 6 faces (see Fig. 3, left-hand part);  $\sum f_f$  = sum of the values of  $f$  at the center of each face;  $\sum f_v$  = sum of the values taken by the function  $f$  at each summit;  $f_m = f(0, 0, 0)$ ;  $h^3$  is the volume of a mesh cube. Since the function to integrate  $f$  must be evaluated at all nodes, it should preferably be an analytical expression. For example if it is intended to compute the force between a sphere  $S$  (with a radius  $R$ ) and an arbitrary volume  $V$  separated by a distance  $z$  (see Fig. 3), the interaction potential  $W_{(dV,S)}$  between the sphere and a volume element  $dV$  of  $V$  should be first computed by integrating equation (2) over the sphere  $S$ , leading to [3]:

$$f \equiv W_{(dV,S)} = \frac{4}{3\pi} \frac{AR^3 dV}{[R^2 - (i^2 + j^2 + k^2)]^3}, \quad (13)$$

where  $A = C\rho_1\rho_2\pi^2$  and  $i, j$  and  $k$  state for the coordinates of the volume element  $dV$ , in the rectangular coordinate frame with its origin located at the center  $O$  of the sphere  $S$  (see Fig. 3b). Of course these coordinates depend on the separation distance  $z$ .

The interaction potential  $W_{(V,S)}(z)$  between a sphere  $S$  and a volume  $V$  separated by a distance  $z$  is consequently (numerically) given by:

$$W_{(V,S)}(z) = \int_V W_{(dV,S)}(z) dV. \quad (14)$$

The force can then be deduced from the energy by applying:

$$F_\eta = -\frac{\partial W}{\partial \eta} = \frac{\partial W}{\partial r} \frac{\partial r}{\partial \eta}, \quad (15)$$

where  $r = \sqrt{i^2 + j^2 + k^2}$  and  $\eta = i, j, k$ . This approach has already been applied by Feddema [28], in order to compute the interaction between a sphere and a rectangular box, in order to propose a handling strategy based on VDW forces.

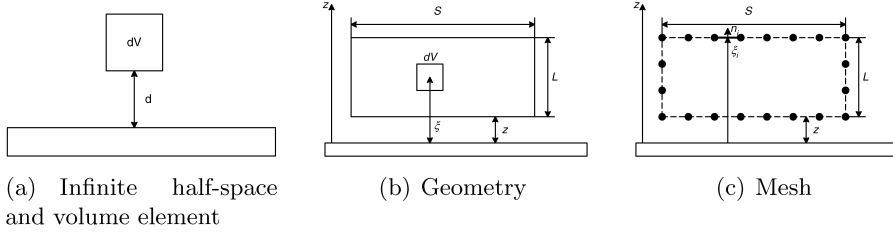


**Figure 4.** Geometry of the rectangular block.

**2.1.4.2. Green identity (divergence theorem)-based integration method.** The VDW force can also be computed by replacing the volume integral by a surface integral using the Green identity [29], as illustrated below with the interaction between an infinite half-space and a rectangular box separated by a distance  $z$  (see Fig. 4b). This problem has an analytical solution that can be used to validate the method. First the interaction potential  $W_{(\text{HS},dV)}$  between an infinite half-space and a volume element  $dV$  located at a distance  $d$  (Fig. 4a) is calculated (both molecular density are equal). Since  $W_{(\text{HS},dV)}(d) = -AdV/(6\pi d^3)$  (see equation (4)), the force  $F$  between the half plane and the rectangular box  $V$  can be calculated by: (1) integrating  $W_{(\text{HS},dV)}(d)$  over the volume  $V$ , located at a distance  $z$  from the HS and (2) derivating this result with respect to  $z$  ( $F(z) = -dW(z)/dz$ ), leading to:

$$F = -\frac{A}{2\pi} \int_V \frac{1}{\xi^4} dV, \quad (16)$$

where  $\xi$  is the position coordinate of the volume element. This integral can be developed as follows:

$$F = -\frac{AS}{2\pi} \int_z^{z+L} \frac{1}{\xi^4} d\xi = \frac{AS}{6\pi} \left( \frac{1}{(z+L)^3} - \frac{1}{z^3} \right). \quad (17)$$

As  $F$  depends on  $A$ ,  $S$  (the section of the rectangular box parallel to the plane, see Fig. 4b),  $L$  (the thickness) and  $z$  (the separation distance between the infinite half-space and the rectangular block),  $F$  is actually written  $F(A, S, L, z)$ . Equation (17) will now be used in combination with the Green identity

$$\int_{\Omega} \int_{\Omega} \int_{\Omega} di v \bar{u} d\Omega = \oint_{\partial\Omega} \bar{u} \cdot \bar{n} d(\partial\Omega).$$

Let us assume a vector field given by  $\bar{u} = -1/(3\xi^3)\bar{1}_z$ . Its divergence is given by  $di v \bar{u} = 1/\xi^4$ . Consequently, equation (16) can now be rewritten as:

$$F(z) = \frac{A}{2\pi} \oint_{\partial V_1} \frac{n_z}{3\xi^3} dS. \quad (18)$$

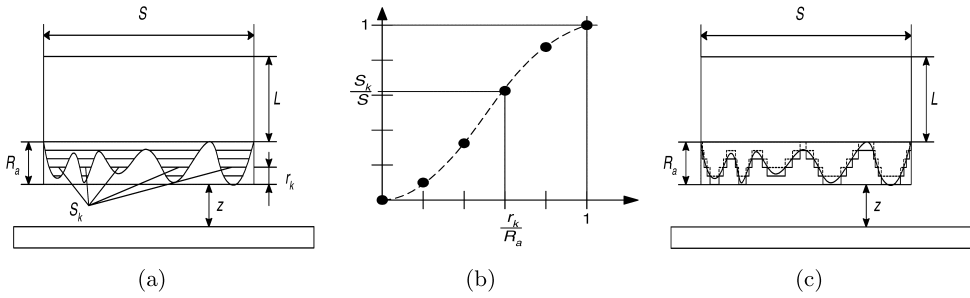


**Figure 5.** (a) Parameters of the rectangular rough block, (b) corresponding Abbott diagram, showing an example of the section ratio as a function of the cut depth and (c) discretized roughness profile.

Then, by meshing the surface of the considered object (see Fig. 4c) into  $N$  surface elements, the  $i$ th element, being characterized by a normal vector with a  $z$ -component  $n_{zi}$ , the integral in equation (18) is replaced by a discrete sum:

$$F(z) = \frac{A}{6\pi} \sum_{i=1}^N \frac{n_{zi}}{\xi_i^3} \Delta S_i. \quad (19)$$

*2.1.5. Applications: roughness and relative orientation.* Let us now assume a rough block placed in front of an infinite half space (see Fig. 5a). The nearest roughness peak is at a distance  $z$  from the plane, and the highest peak is  $R_a$  high. Roughness has been modeled by several authors: Arai [30] only considers the highest roughness peak and assumes that the roughness profile is equivalent to a smooth one, located at a separation distance  $z + (1/2)R_a$  (Fig. 6a). The force given by equation (17) can, thus, be rewritten into:

$$F_{\text{Arai}}(z) = \frac{AS}{6\pi} \left( \frac{1}{\left(z + \frac{R_a}{2} + L\right)^3} - \frac{1}{\left(z + \frac{R_a}{2}\right)^3} \right). \quad (20)$$

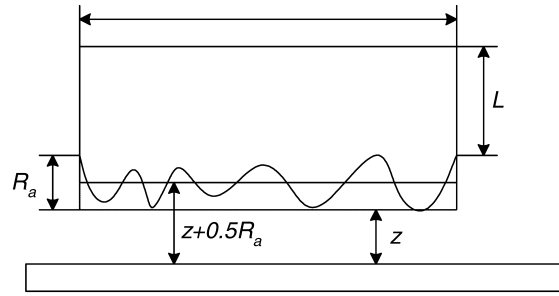
Vögeli [31] assumes that the roughness can be modeled by a profile made of several spheres with a diameter  $R_a$  (see Fig. 6b) leading to the following equation:

$$F_{\text{Vögeli}}(z) = -\frac{AS}{6\pi} \frac{1}{(z + R_a)^3} - \frac{AS}{6\pi z^2 R_a}. \quad (21)$$

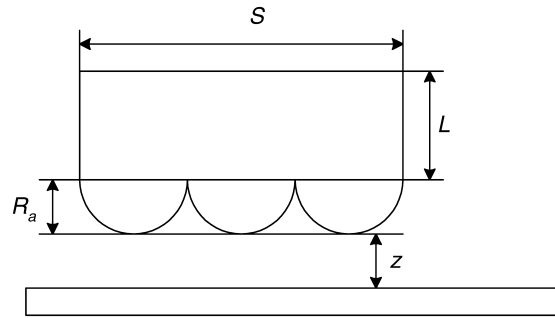
Lambert [32] takes whatever roughness profile into account by considering the Abbott diagram (Fig. 5b) related to the surface, discretizes the roughness profiles into  $M$  cuts (Fig. 5a and 5c) and applies equation (17) to the  $M$  discretized elements:

$$F(z) = F(A, S, L, z + R_a) + \sum_{k=1}^M F(A, S_k, L_k, z + r_k), \quad (22)$$

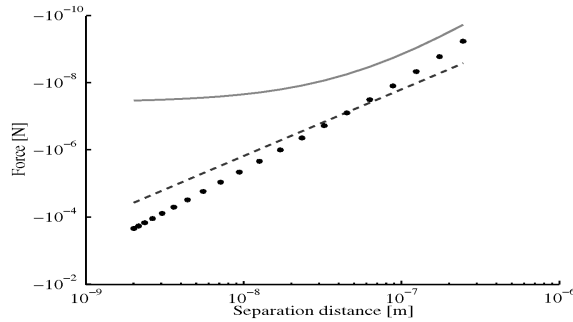
where  $r_k$  is the depth of the  $k$ th cut,  $S_k$  its area and  $L_k$  its thickness ( $L_k = r_k - r_{k-1}$ , see Fig. 5a).



(a)



(b)



(c)

**Figure 6.** (a) Roughness modeled according to Arai [30]; (b) Roughness modeled according to Vögeli [31]; (c) Force (N) as a function of the separation distance (m), with  $R_a = 100$  nm and  $M = 1000$ : continuous line [30]; dashed line [31]; dotted line [32].

The comparison of these models is presented in Fig. 6c for a rectangular block characterized by a section  $S = 20 \mu\text{m} \times 20 \mu\text{m}$ , a height  $L = 10 \mu\text{m}$  and a Hamaker constant  $A_{\text{block}} = 6.5 \times 10^{-20}$  J. The substrate is characterized by  $A_{\text{substrate}} = 30 \times 10^{-20}$  J. The separating medium is assumed to be dry air ( $A_{\text{air}} = 4.5 \times 10^{-20}$  J). From these three Hamaker constants,  $A$  is computed by using the combination law (equation (11)).

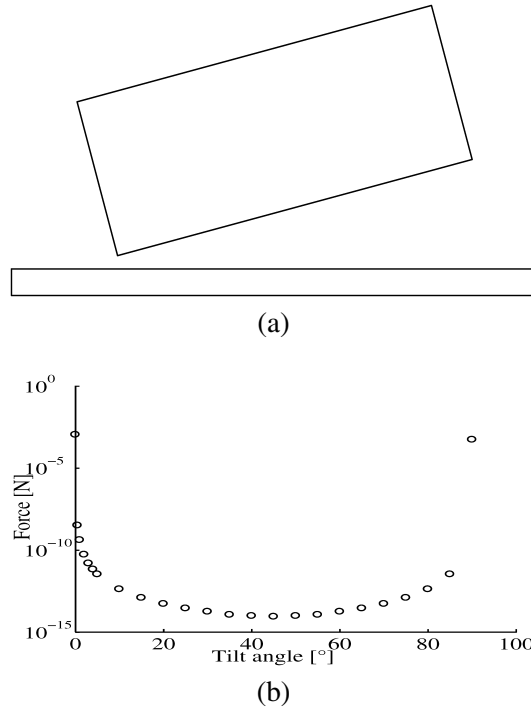


**Figure 7.** (a) Influence of the relative orientation of a smooth rectangular box interacting with an infinite half-space. (b) Force (N) as a function of the separation distance: influence of the tilt angle ( $^{\circ}$ ) on the VDW force at a separation distance of 1 nm.

The case of a tilted box next to an infinite half-space (Fig. 7a) has been treated with the previously presented Green method. It can be seen in Fig. 7b that the force dramatically decreases as soon as the tilt angle becomes different from zero. A handling strategy should consequently aim at modifying the relative angle of only a few degrees between the gripper and the micropart (to release) or between the object and the substrate (to pick up). It is not necessary to tilt the gripper with a  $45^{\circ}$  angle as suggested in Ref. [15], although it is totally exact that the minimum of the force occurs for a  $45^{\circ}$  tilt angle.

*2.1.6. Summary of the approximations and conclusions.* Many expressions of the VDW forces can be found in the scientific literature, corresponding to classical configurations. They are summarized in Table 2: additional references exist about the interaction between a sphere and a cylindrical pore [33], between a sphere and a spherical cavity [34], between two rough planes [35, 36].

It can be concluded that there are several kinds of models: (1) without roughness nor orientation [17, 22]; (2) with roughness but without orientation [30–32]; (3) without roughness but with orientation [15, 32]. Note that we have not found any description of a configuration including both roughness and orientation.

## 2.2. Electrostatic forces

In the previous paragraph, VDW forces were presented. These forces rely mainly on the presence of dipoles which tend to align. This alignment generates a force that is always attractive. Another problem is that the particles tend to be electrostatically charged and the effect of such a charge is significant for a microobject.

*2.2.1. Various interactions.* The electrostatic forces are conventional Coulomb forces. Even if the involved systems are not charged, the triboelectrification involves the creation of surface charge densities [38]. This phenomenon is included in Ref. [39]; thus, different cases can appear.

*2.2.1.1. Interaction charged particle/charged surface and charged particle/charged particle.* In the case of a charged particle  $q$  interacting with a charged surface, the force of interaction is expressed by the law of Coulomb: surface creates a field  $E = \sigma/(2\epsilon\epsilon_0)$  (with  $\sigma$  density of charge,  $\epsilon$  relative permittivity of the medium and  $\epsilon_0$  permittivity of the air). The force is, thus, expressed by:

$$F = qE \quad \text{independently of the distance from separation.} \quad (23)$$

For interactions between charged particles, the Coulomb force is expressed by:

$$F = \frac{q_1q_2}{4\pi\epsilon_0\epsilon r^2}, \quad (24)$$

where  $r$  is the separation distance between the particles.

*2.2.1.2. Interaction charged particle/insulating surface.* When a concentrated charge  $q$  approaches an isolated surface, the force of interaction is expressed by:

$$F = \frac{q^2}{16\pi\epsilon\epsilon_0z^2}, \quad (25)$$

where  $z$  is the distance separating the electrostatic charge and surface, and  $\epsilon$  is the relative permittivity of the medium in which the interaction occurs. For insulating materials characterized by dielectric constants  $\epsilon_1$  and  $\epsilon_2$ , the force is expressed by:

$$F = \frac{q^2}{16\pi\epsilon_1\epsilon_0z^2} \frac{(\epsilon_2 - \epsilon_1)}{(\epsilon_2 + \epsilon_1)} \quad \text{with } \epsilon_2 > \epsilon_1. \quad (26)$$

*2.2.1.3. Interaction between two conductive surfaces.* In the case of two conductive half-spaces separated by a distance  $z$ , the electric field  $E$  is given by:

$$E = \frac{\sigma}{\epsilon\epsilon_0}, \quad (27)$$

and the electrostatic force per unit area is:

$$P = \frac{\sigma E}{2} = \frac{\sigma^2}{2\epsilon\epsilon_0}, \quad (28)$$

This latter expression shows that the electrostatic force (or electrostatic pressure) between plane surfaces does not depend on the separation distance. It only plays a role if the charges distribution is not uniform.

It is very difficult to know the charges distribution (and the resulting electric field) at a microscopic scale. Indeed, the charge distribution on insulating components with a size smaller than  $500 \mu\text{m}$  is not known in advance due to triboelectrification mechanisms.

## 2.2.2. Various contacts.

*2.2.2.1. Conductor–conductor contact.* When two dissimilar materials contact each other, a electron transfer occurs if the separation distance is small ( $\leq 1 \text{ nm}$ ). This transfer brings materials in a thermodynamic balance which tends to equalize their electrochemical potentials. The potential difference between surfaces of the materials 1 and 2, called contact potential difference, is written in the form [40]:

$$V_c = \frac{(\phi_1 - \phi_2)}{e}, \quad (29)$$

where  $\phi_1$  and  $\phi_2$  are the contact potentials of materials 1 and 2. The charge acquired by each material is determined by the condition that to balance, the levels of Fermi of both materials coincide. Therefore, after separation of two materials, the charge  $Q$  of each material can be estimated by [38, 41]:

$$Q = C_0 V_c, \quad (30)$$

with  $C_0$  the capacity at the distance  $z_0$ . The charge  $Q$  is generally about  $Q \approx 10^{-13} \text{ C}$ . This capacity is equal to:

$$C_0 = \frac{\epsilon_0 A_{\text{rea}}}{z_0}, \quad (31)$$

where  $A_{\text{rea}}$  is the contact area and  $z_0$  represents the cut-off separation distance above which no electrons transfer can occur anymore. Consequently, the acquired charge after separation is the one corresponding to a thermodynamic balance at the distance  $z_0$ . For very regular surfaces,  $z_0$  is between  $0.2 \text{ nm}$  and  $0.4 \text{ nm}$  [42].

The experiments undertaken by Lowell and Harper [41, 43] prove that this value maximizes the charge acquired by metals. A value closer to reality is obtained by taking for  $z_0$  the average of roughnesses of two surfaces. As it is not quite obvious to determine, an average value of  $z_0$  is used [43]:

$$z_0 = 100 \text{ nm}.$$

This value of  $z_0$  can be used in various models.

*2.2.2.2. Conductor–insulator contact.* The charge transferred from a conductor to an insulator depends on the work function. This charge is supposed to be given when the levels of Fermi come in coincidence. The calculation of the acquired

charge differs from the previous case and the charge excess within the insulator is not concentrated on surface but in a zone known as the accumulation area, which is generally about the size of the atoms [44].

This charge actually depends on the contact duration, but this one is assumed to be rather long so that thermodynamic balance is reached [45]. The charge density (or the total charge) in an insulator can be calculated starting from the knowledge of the number of electrons occupying the different energy levels of the material [9]. The number  $N_E$  of electrons occupying the energy level  $E_A$  can be determined by the following expression, where  $m$  is the mass of the electron and  $h$  the Planck constant ( $6.626 \cdot 10^{-34} \text{ m}^2 \text{ kg s}^{-1}$ ):

$$N_E = \frac{\pi}{4} \left( \frac{8m}{h^2} \right)^{3/2} E_A^{1/2}, \quad (32)$$

the charge density in the insulator  $\rho$  must satisfy the Poisson equation:

$$\Delta V = -\frac{\rho}{\epsilon_r \epsilon_0}, \quad (33)$$

where  $\rho$  is the charge density,  $V$  the electrostatic potential,  $\epsilon_r$  the dielectric constant of the insulator and  $\epsilon_0$  the dielectric constant of the air.

A solution to this equation is given by [38, 46]:

$$\sigma \approx -\{2\epsilon_r \epsilon_0 n_A kT \exp(-E_A/kT)\}^{1/2} \exp(eV_c/2kT), \quad (34)$$

where  $n_A$  is the density of state, calculated starting from the number of electrons occupying the energy level  $E_A$  (equation (32)) brought back to the volume of material.

This solution assumes that the insulating material only involves densities of states acceptor or donor. Nevertheless, in order to be able to explain the experimental results, it is necessary to assume that the material has densities of states acceptor and donor at the same time. In this case, the surface density of charges is expressed by:

$$\left. \begin{aligned} \sigma &= -\{2\epsilon_r \epsilon_0 n_A E_A V_c\}^{1/2} & V_c \geq 0 \\ \sigma &= +\{2\epsilon_r \epsilon_0 (n_D - n_A) E_A V_c\}^{1/2} & V_c \leq 0 \end{aligned} \right\}, \quad (35)$$

with  $n_A$  and  $n_D$  are density of state, and  $V_c = ((\phi_{\text{conductor}} - \phi_{\text{insulator}})/e) |\sigma|$  generally lies between  $10^{-5} \text{ C m}^{-2}$  and  $10^{-3} \text{ C m}^{-2}$ .

The calculation of  $n_A$  and  $n_D$  is related to the value of energies  $E_A$  and  $E_D$ .  $E_A$  is called energy of ionization and  $E_D$  electronic affinity. Both are physical data of materials.

**2.2.2.3. Insulator–insulator contact.** There are many experiments to suggest that the contact insulator-insulator is caused by the same mechanism as the preceding contact. Nevertheless, the main phenomenon for this contact is a mechanism of transfer of ions and not of electrons [38].

The potential energy of an ion varies with its position between two very close surfaces. This potential includes the densities of surface charge previously deposited. With balance, the ions concentrate close to the minimum of adjacent potential on these surfaces. The relationship between the density of ions  $n_1$  and  $n_2$  each surface is given by:

$$\frac{n_1}{n_2} = \exp\left(\frac{-\Delta U}{kT}\right) \quad \text{with} \quad \Delta U = U_2 - U_1, \quad (36)$$

the densities of ions are generally physical data of material. Therefore, equation (36) is used to determine  $\Delta U$ . If the potentials  $U_1$  and  $U_2$  are significant compared to  $kT$ , and by considering the electric field equal to  $\delta U/z$ , the density of electrostatic charge  $\sigma$  is expressed by:

$$\sigma = \frac{\epsilon_0 \Delta U}{ez} \quad \sigma \in [10^{-5} \text{ C m}^{-2} - 10^{-3} \text{ C m}^{-2}], \quad (37)$$

with  $\Delta U$  very near to 1 eV. If the two insulators are identical, the transfer of charges exists but is weak (about  $10^{-5} \text{ C m}^{-2}$ ).

### 2.3. Capillary forces

*2.3.1. Origin of the capillary forces.* Basically, the capillary forces arise in two ways: either a liquid drop is put between two solids (e.g., a gripper and a component) and turns itself towards a meniscus (= a liquid bridge), or a capillary bridge appears by condensation of the ambient humidity in the small cracks and pores made by two roughness profiles brought in contact (e.g., in a surface force apparatus [47, 48] or during MEMS working or manufacturing [49]).

In both cases, the situation can be described (see Fig. 8a) by a liquid bridge characterized by a volume  $V$ , a surface tension  $\gamma$  and wettability properties defined by the contact angles  $\theta_1$  and  $\theta_2$ . According to the Young–Dupré equation [22], the contact angle  $\theta_i$  is given by:

$$\cos \theta_i = \frac{\gamma_{\text{SV}_i} - \gamma_{\text{SL}_i}}{\gamma}, \quad (38)$$

where  $\gamma_{\text{SL}_i}$  ( $\gamma_{\text{SV}_i}$ ) states for the interfacial energy between the solid  $i$  and the liquid (vapor). The force exerted by the meniscus on a solid has two contributions: according to Ref. [47], the term ‘capillary force’ refers to the force due to the pressure difference  $\Delta p$  ( $\Delta$  is not the Laplacian operator in this case) across the curved liquid–fluid interface. Depending on the sign of  $\Delta p$ , it can be attractive or repulsive, as shown by the Laplace equation [22]:

$$\Delta p = p_{\text{in}} - p_{\text{out}} = 2\gamma H, \quad (39)$$

where  $H$  is the mean curvature of the liquid–vapor (LV) interface, defined as:

$$H = \frac{1}{2} \left( \frac{1}{\rho'} - \frac{1}{\rho} \right), \quad (40)$$

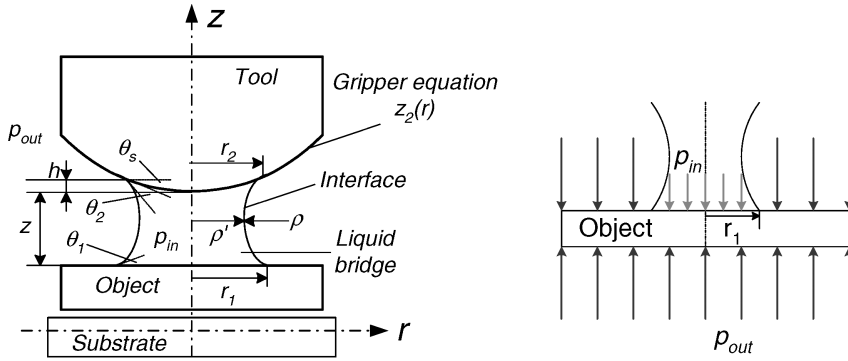


**Figure 8.** (a) Curved solid (gripper, AFM tip) linked to a flat solid (component, substrate) by a liquid bridge. (b) Origin of the ‘capillary force’ (attractive case).

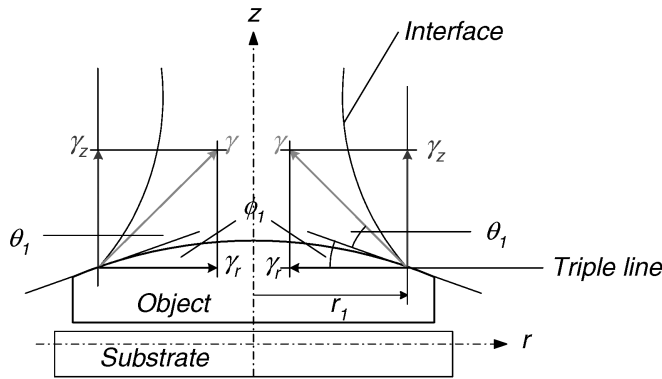


**Figure 9.** Origin of the ‘interfacial tension force’: the force directly exerted by the liquid interface on the solid surface must be projected on the vertical direction, the radial components balancing each other.

where  $\rho$  is the main curvature radius of the interface in the plane containing the symmetry axis  $z$  and  $\rho'$  is the main curvature radius in the plane perpendicular to this symmetry axis. Note that in Fig. 8a,  $\rho'$  is positive while  $\rho$  is negative.

As  $\Delta p$  acts over an area  $\pi r_1^2$ , the capillary force  $F_L$  is given by:

$$F_L = 2\gamma H \pi r_1^2. \tag{41}$$

The term ‘interfacial tension force’ implies the force directly exerted by the liquid interface on the solid surface. As illustrated in Fig. 9, the surface tension  $\gamma$  acting along the contact circle must be projected on the vertical direction, leading to:

$$F_T = 2\pi r_1 \gamma \sin(\theta_1 + \phi_1). \tag{42}$$

Therefore, the total capillary forces exerted on the solid are given by:

$$F_C = F_L + F_T = 2\gamma H \pi r_1^2 + 2\pi r_1 \gamma \sin(\theta_1 + \phi_1). \tag{43}$$

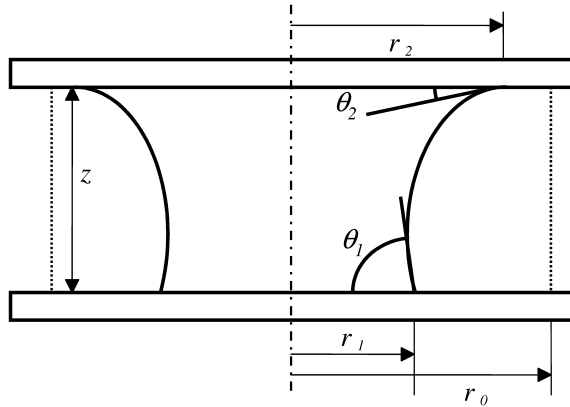


**Figure 10.** Example of the ‘potential’ method: case of two parallel plates.

Note that several authors only consider the ‘capillary’ term [47, 50], while others only consider the ‘interfacial tension’ term [51]. According to Refs [52–54], we will take both parts into account.

*2.3.2. State of the art of the approximations.* Most often the capillary forces are approximated by several formulations that all include the following assumptions: (1) axial symmetry of the liquid bridge, (2) gravity effects on the meniscus shape are neglected (in other words, a vanishing Bond number  $B_0 = (\rho g L^2)/\gamma$  ( $L$  is the meniscus height) is assumed, which means a meniscus with a size smaller than the capillary length  $L_C = \sqrt{\gamma/(\rho g)}$ , where  $g$  is the gravity acceleration,  $\gamma$  the surface tension of the liquid–vapor interface and  $\rho$  is the liquid density; actually it should be written  $\Delta\rho = \rho_{\text{liquid}} - \rho_{\text{vapor}}$ , but the density of air can be neglected compared to that of water).

The main approaches are [3]:

1. To compute the force by derivating a potential  $W$  with respect to the gap  $z$  between the two objects at apex (see Fig. 8a for  $z$ ):

$$F = -\frac{dW}{dz}. \quad (44)$$

This approach is illustrated by the case of two parallel plates linked by a meniscus, as represented in Fig. 10a. The system has three phases, three interfaces leading to a total energy equal to:

$$W = W_{\text{SL}} + W_{\text{SV}} + W_{\text{LV}} = \gamma_{\text{SL}}S_{\text{SL}} + \gamma_{\text{SV}}S_{\text{SV}} + \gamma S_{\text{LV}}, \quad (45)$$

where  $W_{\text{SL}} = \gamma_{\text{SL}1}\pi r_1^2 + \gamma_{\text{SL}2}\pi r_2^2$ ,  $W_{\text{SV}} = \gamma_{\text{SV}1}(\pi r_0^2 - \pi r_1^2) + \gamma_{\text{SV}2}(\pi r_0^2 - \pi r_2^2)$  and  $W_{\text{LV}} = \gamma S$ . In these equations,  $r_0$  is an arbitrary constant radius, larger than the maximum between  $r_1$  and  $r_2$ : it only helps to express the solid–vapor interface area and vanishes when deriving  $W$  in the next equation.  $S$  is the area

of the liquid–vapor interface (the lateral area of the meniscus).

$$F = -\frac{dW}{dz} = -\gamma_{SL1}2\pi r_1 \frac{dr_1}{dz} - \gamma_{SL2}2\pi r_2 \frac{dr_2}{dz} + \gamma_{SV1}2\pi r_1 \frac{dr_1}{dz} + \gamma_{SV2}2\pi r_2 \frac{dr_2}{dz} - \gamma \frac{dS}{dz}. \quad (46)$$

In order to calculate all the derivatives involved in this expression, additional assumptions must be stated: (1) the volume of the meniscus remains constant, (2) the separation distance  $z$  is small compared to the radius  $r_1$  and  $r_2$ : henceforth, we neglect the term depending on the lateral area  $S$ , (3) the liquid volume can be approximated by  $V \approx \pi r_1^2 z$ , leading to  $dr_1/dz = -r_1/2z$ , (4) in the same way,  $dr_2/dz = -r_2/2z$ .

With these assumptions, equation (46) can now be rewritten as:

$$F = -\frac{\pi\gamma}{z}(r_1^2 \cos \theta_1 + r_2^2 \cos \theta_2), \quad (47)$$

or, in the case of two plates made of the same material  $F = -(2\pi\gamma/z)r^2 \cos \theta$ . If the liquid–vapor area is assumed to be approximatively equal to  $S \approx 2\pi r z$ , then it can be shown that:

$$F = -\frac{2\pi\gamma}{z}r^2 \cos \theta - \pi r \gamma, \quad (48)$$

or, by replacing the radius by  $r = \sqrt{V/\pi z}$ :

$$F = -\frac{V\gamma \cos \theta}{z^2} - \gamma \sqrt{\frac{\pi V}{z}}. \quad (49)$$

The sign ‘–’ indicates that the energy increases ( $dA/dz > 0$ ) when the plates are pulled away from each other. Consequently, the force is attractive.

2. To assume that the meniscus shape can be approximated by:

(a) A circle [47, 48]:  $(r - r_0)^2 + (z - z_0)^2 = \rho^2$  ( $\rho$  stands for the circle radius,  $r_0$  and  $z_0$  for the coordinates of its center);

(b) A parabola [54]:  $r = az^2 + bz + c$ .

These profiles allow to feed equation (43) with the required geometrical data. In Ref. [54] it is concluded that the circle approximation (also called ‘toroidal’ approximation) ‘is the more difficult to use since the radius  $\rho$  passes through infinity as the bridge changes from a convex to concave geometry’.

3. To numerically compute the shape  $r = r(z)$  of the meniscus by writing the differential formulation of the curvature  $H$  of an axially symmetrical surface [52, 55]:

$$H = \frac{r''}{(1 + r'^2)^{\frac{3}{2}}} - \frac{1}{r(1 + r'^2)^{\frac{1}{2}}} = \frac{p_{in} - p_{out}}{2\gamma}, \quad (50)$$

where  $()' = d()/dz$ .

2.3.3. *Boundary conditions.* Except in the case of the energetic method (method 1), the geometrical methods (circle and parabola) and the differential formulation (method 3) require boundary conditions to be used. For example, in the circle approximation, three parameters must be determined: the coordinates of the center  $r_0$  and  $z_0$  and the radius  $\rho$  (the parameters  $a, b, c$  in the case of the parabola). The corresponding conditions that are imposed are that the meniscus shape must respect the contact angles on both solids (two conditions) and the third condition is provided either by the volume of liquid in the case of a given droplet put between two solids or by the curvature  $H$  in the case of a capillary condensation problem, this curvature being given by the so-called Kelvin equation [22]:

$$(2H)^{-1} = r_k = \frac{\gamma v}{RT \log \frac{p_0}{p}}, \quad (51)$$

where  $v$  is the molar volume of the liquid,  $R$  is the perfect gas constant,  $T$  is the absolute temperature,  $p_0/p$  is the relative vapor pressure (= relative humidity for water). Israelachvili [17] gives  $\gamma v/(RT) = 0.54$  nm for water at  $20^\circ$ . This method has been used by Stifter *et al.* [48].

When solving equation (50), the radius of the contact circle of the meniscus along the upper solid (gripper) is guessed (and referred to as ‘starting point’ in Fig. 11) and the corresponding contact angle is immediately satisfied. There are still two conditions to impose (the second contact angle and either  $\Delta p$  or the volume of liquid). As equation (50) can only be solved if  $\Delta p$  and the ‘starting point’ are known, an iterative scheme should be achieved: (1) in the capillary condensation problem,  $\Delta p$  is given by the Laplace equation ( $\Delta p = 2H\gamma$ ) in which the curvature is determined by the Kelvin equation (equation (51)) and the starting point of the meniscus along the first solid is adjusted in an iterative way so that the contact angle on the second solid is satisfied; (2) in the case of a given volume of liquid,  $\Delta p$  can be adjusted so that the contact angle is respected [52] and the starting point is adjusted to fit the volume of liquid [55]. This double iterative scheme is graphically illustrated in Fig. 11. More details on the results obtained by this method can be found in Ref. [3].

2.3.4. *Conclusions.* As a conclusion to this subsection, let us remind that we presented analytical and numerical algorithms to compute capillary forces. The originality of the numerical exposed method lies in the fact that the volume of liquid is considered an input parameter.

Table 3 summarizes several classical approximations found in the literature and gives the corresponding references and assumptions (see Fig. 8a):

1. parallel plates;
2. spherical tip (radius  $R$ ) near a plate;
3. arc approximation of the interface (where  $\rho = \text{constant}$  is the radius);
4. potential formulation;

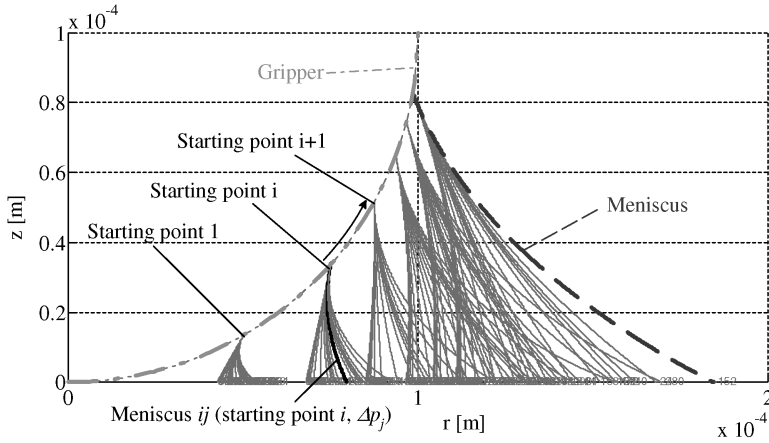


**Figure 11.** Graphical illustration of the double iterative scheme for a spherical gripper ( $R = 0.1$  mm), water,  $\theta_1 = \theta_2 = 30^\circ$ ,  $V = 4.5$  nl,  $z = 0$ . Meniscus  $ij$  is obtained with the  $i$ th starting point and the  $j$ th pressure difference.

**Table 3.**

Summary of the capillary forces

| Ref.          | Force   | Assumptions        |
|---------------|---|--------------------|
| [47]          | $F = 4\pi R\gamma \cos \theta$  | 2, 5, 6, 7, 8, 9   |
| [47]          | $F = 4\pi R\gamma \cos \theta \frac{1}{2} \left( \frac{(r_1/R)^2}{z/R+1-(1-(r_1/R)^2)^{1/2}} - \frac{r_1/R}{4 \cos \theta} \right)$ | 2, 3, 6, 7, 16     |
| Equation (47) | $F = \frac{\pi\gamma}{z} (r_1^2 \cos \theta_1 + r_2^2 \cos \theta_2)$   | 1, 4, 7, 8, 10, 11 |
| Equation (48) | $F = \frac{2\pi\gamma}{z} R^2 \cos \theta + \pi R\gamma$  | 1, 4, 7, 8, 11, 12 |
| [17]          | $F = \frac{4\pi R\gamma \cos \theta}{1+(z/h)}$  | 2, 4, 7, 13, 14    |
| [48]          | $F = \pi\gamma\rho'^2 \left( \frac{1}{\rho} - \frac{1}{\rho'} \right)$  | 2, 3, 15           |
| [56]          | $F = 2\pi\gamma\rho' + \frac{\gamma}{\rho}\pi\rho'^2$   | 1, 3, 8, 9         |
| [57]          | $F = 2\pi\gamma\rho' + \frac{\gamma}{\rho}\pi \frac{z}{2\sin \theta}$   | 1, 3, 7, 9         |
| [52]          | $F = 2\pi r_1\gamma \sin(\theta_2 + \theta_s) + \pi r_1^2\gamma \left( \frac{1}{\rho} - \frac{1}{r_1} \right)$                      | 2, 3               |

5. the radii  $r_1$  and  $r_2$  of the two circular contact lines are very small compared to  $R$ ;
6.  $r_1 = r_2 = r$  ('symmetric case');
7. the contact angles are equal  $\theta_1 = \theta_2 = \theta$ ;
8. the gap  $z$  is very small compared to the radius  $r$  of the contact line;
9. the curvature of the interface in the horizontal plane is negligible  $|\frac{1}{\rho'}| \ll |\frac{1}{\rho}|$ ;
10. contribution of the interfacial energy liquid–vapor is neglected;
11. constant volume  $V \approx \pi r_1^2 z$ ;
12. interfacial area liquid–vapor  $S \approx 2\pi r_1 z$ ;

13. constant volume  $V = V_{\text{cylindre}} - V_{\text{sphere}} \approx \pi R^2 z \theta_s^2 + \frac{\pi}{4} R^3 \theta_s^4$  ( $\theta_s \approx 0$ );
14. immersion height  $h$  is small ( $\theta_s \approx 0$ );
15. interfacial tension force is neglected.

Capillary forces are very important in miniaturized systems because of the scaling laws: this kind of force is linear with the size of the system, i.e., their relative importance compared to the weight becomes 100-times larger for a 10-times reduced system. Note that these forces are particularly important in bubble microfluidic systems, i.e., when there are liquid–vapor interfaces (they are less important in flows occurring inside microchannels).

### 3. CONTACT FORCES

When contacting, two surfaces are subject to deformation and adhesion, the latter being characterized by the so-called pull-off force, required to separate these two surfaces. In the same way, the microscopic friction will play a dominating role for the strategies of microhandling. Therefore, it is necessary to understand the main properties of the surfaces in contact.

#### 3.1. Deformations

The adhesion forces deal with the interfaces between surfaces in contact. No solid being completely rigid, the action of these forces consequently increases the contact area due to the deformation of the solids. In order to quantify the role of these forces in a system, it is essential to describe the deformations taking place, which depend on the elastic and viscoelastic properties of materials, their roughness, the surface forces and the external applied load.

From the point of view of micromanipulation, the deformations of the objects play two roles: (i) they increase surfaces of interaction and consequently the module of adhesion forces and (ii) they introduce a new force known as ‘pull-off’ (or separation) which is necessary to separate two solids initially in contact.

Several models describe the deformations. The first one (proposed in 1895 by Hertz) considers a set of two perfectly elastic spheres in contact by assuming an interaction without any attraction nor adhesion and a repulsion between two surfaces [58–60]. For spheres with radii  $R_1$  and  $R_2$ , Young moduli  $E_1$  and  $E_2$  and Poisson’s ratios  $\nu_1$  and  $\nu_2$ , this theory leads to the radius of the contact area  $a$ , given by:

$$a^3 = \frac{RF_{\text{ext}}}{K}, \quad (52)$$

where

$$\frac{1}{K} = \frac{3}{4} \left( \frac{1 - \nu_1^2}{E_1} + \frac{1 - \nu_2^2}{E_2} \right) \quad \text{and} \quad \frac{1}{R} = \frac{1}{R_1} + \frac{1}{R_2}.$$

The deformation then leads to an indentation  $\delta$  (i.e., the centers of the spheres are separated from  $R_1 + R_2 - \delta$ ) calculated by the following expression:

$$\delta = \frac{a^2}{R} = \frac{F_{\text{ext}}}{Ka}. \quad (53)$$

This model, however, is not adapted to the description of the deformations on a microscopic scale since it does not integrate any effect of adhesion. Nevertheless, it was used as a basis for the development of the following models.

In 1971 Johnson, Kendall and Roberts (JKR) [61], noted that for low-weight spheres, the contact area is clearly underestimated by the Hertz model and that strong adhesion forces keep surfaces in contact when they are clean and dry. The Hertz model remains valid for larger spheres, when the adhesion forces become negligible compared with the weight.

These authors then proposed a theory derived from Hertz's, on the basis of two spheres which adhere when they come into contact. The JKR model describes the contact area by:

$$a^3 = \frac{R}{K} \left\{ F_{\text{ext}} + 3\pi RW_{12} + \sqrt{6\pi RW_{12}F_{\text{ext}} + (3\pi W_{12}R)^2} \right\}, \quad (54)$$

and the indentation  $\delta$  by:

$$\delta = \frac{a^2}{R} - \sqrt{\frac{8\pi W_{12}a}{3K}}. \quad (55)$$

These two formulas take into account the effects of adhesion between the bodies 1 and 2. When  $W_{12}$  is null, the contact area is identical to the one described by the Hertz model. If the external load vanishes the radius  $a_0$  of the contact area is:

$$a_0^3 = \frac{6\pi W_{12}R^2}{K}.$$

This contact area generates adhesion forces which have to be overcome in order to separate two objects initially in contact. Still according to this theory, it is therefore necessary to apply for this purpose a negative load  $P$  called 'pull-off' or separation force expressed by:

$$P = -\frac{3}{2}\pi RW_{12}. \quad (56)$$

From a theoretical point of view, this model presents an anomaly. Indeed it considers an infinite tension at the edge of the contact area. In 1975 Derjaguin, Muller and Toporov (DMT) [62] proposed a theory between the two previous ones in order to avoid this infinite tension by considering a Hertzian deformation of the contact area and an adhesion. According to this latter theory the force required to separate the solids is expressed by:

$$P = -2\pi RW_{12}. \quad (57)$$

The determination of the deformations and the contact area has been widely studied to validate either theory. The transition between the DMT and JKR models has been studied by Mangis [63], who introduced the parameter  $\lambda$  called elasticity parameter. This parameter can be expressed by

$$\lambda = 2\sigma_0 \left( \frac{R}{\pi W K^2} \right)^{1/3}, \quad (58)$$

where  $\sigma_0 = W/h$  and  $h \approx 1$  ( $\lambda \rightarrow 0$ : DMT,  $\lambda \rightarrow \infty$ : JKR).

Contact parameters,  $a$  and  $\delta$ , are obtained by the simultaneous resolution of the system of three equations with three unknowns:

$$1 = \frac{\lambda a^2}{2} \left( \frac{K}{\pi W R^2} \right)^{2/3} \left( (m^2 - 2) \arctan \sqrt{m^2 - 1} + \sqrt{m^2 - 1} \right) + \frac{4\lambda^2 a}{3} \left( \frac{K}{\pi W R^2} \right)^{1/3} \left( \sqrt{m^2 - 1} \arctan \sqrt{m^2 - 1} - m + 1 \right), \quad (59)$$

$$F = \frac{K a^3}{R} - \lambda a^2 \left( \frac{K}{\pi W R^2} \right)^{1/3} \left( \sqrt{m^2 - 1} + m^2 \arctan \sqrt{m^2 - 1} \right), \quad (60)$$

$$\delta = \frac{a^2}{R} - \frac{4\lambda a}{3} \left( \frac{\pi W}{K R} \right)^{1/3} \sqrt{m^2 - 1}. \quad (61)$$

The pull-off force is then expressed by:

$$P = -2\sigma_0 a^2 \left( m^2 \arctan \sqrt{m^2 - 1} + \sqrt{m^2 - 1} \right). \quad (62)$$

This system seems rather complex to solve [64]. A generalized and simplified formulation of these equations was given in Ref. [65], writing the pull-off force by:

$$P = -\frac{1}{4} \left( 7 - \frac{4.04\lambda^{1/4} - 1}{4.04\lambda^{1/4} + 1} \right) \pi W R, \quad (63)$$

and the contact radius by

$$\frac{a}{a_0} = \left( \frac{\alpha + \sqrt{1 + F/F_{\text{adh}}(\alpha)}}{1 + \alpha} \right)^{2/3}, \quad (64)$$

with

$$a_0 = \left( 1.54 + 0.279 \frac{2.28\lambda^{1/3} - 1}{2.28\lambda^{1/3} + 1} \right) \left( \frac{\pi W R^2}{K} \right)^{1/3} \quad \text{et } \lambda = -0.924 \ln(1 - 1.02\alpha).$$

These empirical equations form a more practical solution than the Maugis solution with less than 1% of error. These equations could, thus, be used in

micromanipulation models. Model selection can then be summarized in the following way according to  $\lambda$  coefficient:

$$\begin{aligned} \lambda < 0.1 & \quad \text{DMT model} \\ 0.1 < \lambda < 5 & \quad \text{Dugdale model using Carpick interpolation} \\ \lambda > 5 & \quad \text{JKR model.} \end{aligned}$$

These formulas use the surface energy whose definition and principal properties are proposed in what follows.

### 3.2. Interaction energy of two bodies

*3.2.1. Adhesion and cohesion works.* These works represent the energy required per unit area to separate two media from contact to infinity (in vacuum). This energy is called the work of adhesion ( $W_{12}$ ) for two different media and work of cohesion ( $W_{11}$ ) for two identical media.

*3.2.2. Surface energy and tension force.* The surface energy  $\gamma$  represents the energy needed to increase the free surface of one unit area. Since it consists in separating two surfaces initially in contact, it is equal to half the cohesion work:

$$\gamma_1 = \frac{1}{2} W_{11}.$$

For solids, it is noted  $\gamma_s$  and is regarded as an energy per unit of area, usually  $\text{mJ m}^{-2}$ . For liquids it is noted  $\gamma_l$  or  $\gamma$  and is given like a tension force per unit length, usually  $\text{mN m}^{-1}$ . This energy of surface often depends on the boiling point. Consequently, substances like metals which have a high boiling point ( $T > 2000^\circ\text{C}$ ) have significant surface energies ( $\gamma > 1000 \text{ mJ m}^{-2}$ ).

*3.2.3. Interfacial energy.* When two media are in contact, the energy of their interface (by unit area) is noted interfacial energy or interfacial tension  $\gamma_{12}$ , and given by:

$$\gamma_{12} = \frac{1}{2} W_{11} + \frac{1}{2} W_{22} - W_{12} = \gamma_1 + \gamma_2 - W_{12}.$$

This equation is called Dupré equation (see also equation (38)). The relation of the combination between  $\gamma_{12}$  and  $\gamma_1, \gamma_2$  is obtained by starting from a thermodynamic approach explained in Ref. [17]:

$$\gamma_{12} = \gamma_1 + \gamma_2 - 2\sqrt{\gamma_1 \gamma_2}.$$

*3.2.4. Work of adhesion in a third medium.* From the previous formulas the energy  $W_{132}$  required to separate two media 1 and 2 immersed in a medium 3 is given by:

$$W_{132} = W_{12} + W_{33} - W_{13} - W_{23} = \gamma_{13} + \gamma_{23} - \gamma_{12}.$$

### 3.3. Transition between surface forces and contact forces

The interaction potential (= interaction energy) of van der Waals between two parallel planes being given by equation (6), the energy required to increase the separation distance from  $z = z_0$  to  $z = \infty$  can be expressed as follows:

$$\Delta W = W_{(p,p)}(z = \infty) - W_{(p,p)}(z_0) = \frac{A}{12\pi z_0^2}. \quad (65)$$

As the surface energy is half the energy required to separate two media from contact to infinity, the work  $\Delta W$  can also be deduced from:

$$\Delta W = -W_{(p,p)}(z_0) = 2\gamma \Rightarrow \gamma = \frac{A}{24\pi z_0^2} \text{ per unit area.} \quad (66)$$

This equation provides the link between the surface energy and the Hamaker constant. Note that the value of  $z_0$  is still to be determined: at first sight, the average distance between atoms (0.4 nm) could be judiciously used. Nevertheless, the experiments showed that this choice largely underestimates  $\gamma$  [17]. The main reason therefore lies in the fact that the expression of  $W_{(p,p)}(z)$  is obtained by a continuous medium approach, while a quantum approach is more suitable since the contact distance is of the same order of magnitude as molecular dimensions. Nevertheless, this can be corrected empirically by dividing  $z_0$  by a correction factor, equal to 2.5, leading to replace  $z_0$  by 0.165 nm. The choice of this value allows the good correlation between the theoretical and experimental values of  $\gamma$  and  $A$  [17].

$$\gamma = \frac{A}{24\pi(0.165)^2} \quad A = 2.1 \times 10^{-21}\gamma. \quad (67)$$

A corrected expression  $W_{(p,p)}^c$  of  $W_{(p,p)}$  is then given by:

$$W_{(p,p)}^c(D_0) = -\frac{A}{12\pi(z_0/2.5)^2}. \quad (68)$$

It should be noted that this approximation provides correct results for most materials, but that it largely underestimates the value of  $\gamma$  in the case of strongly polar materials or metals for which it is preferable to use experimental values. If the calculation of the VDW forces were based on the constants of Hamaker and not on the experimental expressions of the energy of surface, it would become necessary to integrate this correction in the expression of  $W_{(p,p)}(z)$ . A significant discontinuity would then appear in the estimation of this potential. A second point is that a discontinuity appears in models between surface forces and contact forces.

### 3.4. Friction

Friction also seems to be a significant physical phenomenon for micromanipulation. From a macroscopic point of view, friction leads to a (friction) force which is

opposed to the motion direction. Its expression, according to the classical Coulomb model, is then:

$$F_{\text{fric}} = \mu F_{\text{ext}},$$

where  $\mu$  is the friction coefficient.

At the microscopic scale, it is necessary to consider friction phenomena between surfaces in static and slipping contact (in presence or not of lubricant). Tabor [66] draws up a state of the art of the processes of friction on a considered scale, in absence of lubrication. He points out three things:

- (i) the contact area: it depends on the topography of surfaces and the characteristics of materials in contact. Although good ideal models exist, this determination is limited by the lack of reliable experimental methods taking into account the slipping contact and some other surfaces phenomena (oxidation, state of the microasperities, etc.);
- (ii) the action of the interfacial connections, like the van der Waals forces or the metal connections (by exchanges of electrons): they increase the coefficient of friction  $\mu$  up to high values (several times the unit). However, this effect is compensated by the phenomena of oxidation which lead to surface films and, hence, to a considerable decrease of the friction coefficient ( $\mu \approx 0.1$ );
- (iii) the problems of deformations during sliding: they create a ‘tilling’ surface, increasing the friction coefficient.

Consequently, it clearly turns out that the action of the adhesion forces and the presence or absence of lubricant are dominating factors for the quantification of the friction forces.

Many measurements carried out with the AFM are related to the frictional properties of various materials. These studies lead to the characterization of these properties by measuring either the shear stress  $\tau$  or the coefficient of friction  $\mu$ . The low dimension of surfaces leads to a mono-asperity contact, which means the force of friction  $f$  is proportional to the contact area  $a$ . Thus, the force of friction is written [31]:

$$F = \tau \pi a^2. \quad (69)$$

The contact area can be estimated from the previous theories, JKR, Dugdale or DMT. An estimation of the force of friction can, thus, be made.

There is another approach which establishes that the macroscopic approach can be applied to these forces of adhesion to determine the force of friction. The macroscopic approach can be applied to these adhesion forces to algebraically determine the force of friction. Indeed, they can be regarded as external forces since pull-off forces characterize the influence of a surface on the other one. Within this framework, this friction force is expressed by Ando and Ino [67]:

$$F_{\text{fric}} = \mu(F_{\text{adh}} + F_{\text{ext}}), \quad (70)$$

where  $\mu$  is the coefficient of friction. This expression is also true for  $F_{\text{ext}} < 0$  [68].

#### 4. CONCLUSIONS

In this study several models have been summarized, from surface forces to contact forces. By applying these models to our case studies, we conclude as follows: (1) due to the roughness of small manufactured parts, it turns out from this study that van der Waals forces can be neglected compared to other forces like capillary forces. Moreover, the influence of these forces can be reduced if needed by tilting the gripper. (2) A study of the capillary forces for use as a gripping principle has proved the suitability of this principle to pick up components (several mN near contact) and pointed out several release strategies: evaporation of the liquid bridge, control of adhesion by electrowetting. (3) Due to its importance, pick-up strategies have also been proposed to take benefit from the pull-off force [69]. In this latter case, release is ensured by applying an important acceleration to the gripper [70].

As future works, the handling strategies based on the pull-off and capillary forces should be improved and actual gripper prototypes should replace the experimental set ups that have been designed to validate the principles.

#### REFERENCES

1. B. J. Nelson, Microassembly and its applications, in: *Proc. of Symposium of Mechatronics and Microsystems*, p. 59, TU Delft (2003).
2. B. J. Nelson, Microassembly processes and microassembled devices: Which comes first? in: *Proc. of the International Symposium on Assembly and Task Planning*, Keynote speech, Montreal (2005).
3. P. Lambert, A contribution to microassembly: a study of capillary forces as a gripping principle, PhD thesis, Université Libre de Bruxelles, Brussels (2004).
4. J. Peirs, Design of micromechatronic systems: scale laws, technologies, and medical applications, PhD thesis, KUL Leuven, Leuven (2001).
5. M. Tichem, B. Karpuschewski and P. M. Sarro, Self-adjustment of micro-mechatronic systems, *CIRP Annals* (2003).
6. S. Saito, H. Miyazaki and T. Sato, Micro-object pick and place operation under sem based on micro-physics, *Journal of Robotics and Mechatronics* **14** (3), 227–237 (2002).
7. V. Vandaele, P. Lambert and A. Delchambre, Non-contact handling in microassembly: acoustical levitation, *Precision Engineering* (2006) (in press).
8. F. Bourgeois and J. Jacot, Comprendre le chassage à l'échelle horlogère, in: *Actes des Journées de Chronométrie*, Montreux (2004).
9. L. H. Lee, *The Chemistry and Physics of Solid Adhesion*, in *Fundamentals of Adhesion*. Plenum Press, New York, NY (1991).
10. R. A. Bowling, A theoretical review of particle adhesion, in: *Symposium on Particles on Surface I: Detection, Adhesion and Removal*, San Francisco, pp. 129–142 (1986).

11. R. S. Fearing, Survey of sticking effects for micro parts handling, in: *Proc. of the IEEE/RSJ Intelligent Robots System*, pp. 212–217 (1995).
12. M. Gauthier, B. Lopez-Walle and C. Clévy, Comparison between micro-objects manipulations in dry and liquid mediums, in: *Proc. of CIRA*, Finland (2005).
13. L. Benmayor, Dimensional analysis and similitude in microsystem design and assembly, PhD thesis, Ecole Polytechnique Fédérale de Lausanne, Lausanne (2000).
14. F. Arai and T. Fukuda, A new pick up and release method by heating for micromanipulation, in: *IEEE Workshop on Micro Electro Mechanical Systems*, Nagoya, pp. 383–388 (1997).
15. J. T. Feddema, P. Xavier and R. Brown, Micro-assembly planning with van der Waals force, in: *Proc. of IEEE Int. Symposium on Assembly and Task Planning*, Porto, pp. 32–38 (1999).
16. J. N. Israelachvili, The nature of van der waals forces, *Contemp. Phys.* **15** (2), 159–177 (1974).
17. J. N. Israelachvili, *Intermolecular and Surface Forces*, 2nd edn. Academic Press, San Diego, CA (1992).
18. F. London, The London–van der Waals attraction between spherical particles, *Physica* **4** (10), 1058–1072 (1937).
19. W. B. Russel, D. A. Saville and W. R. Schowalter, *Colloidal Dispersions*. Cambridge University Press, Cambridge (1989).
20. H. B. C. Casimir and D. Polder, The influence of retardation of the London–van der Waals forces, *Phys. Rev.* **73** (4), 360 (1948).
21. E. Lifshitz, The theory of molecular attractive forces between solids, *Soviet Phys.* **2**, 73–83 (1956).
22. A. W. Adamson and A. P. Gast, *Physical Chemistry of Surfaces*, 6th edn. Wiley, New York, NY (1997).
23. H. C. Hamaker, The london van der waals attraction between spherical particles, *Physica* **10**, 1058–1072 (1937).
24. Y. Rollot, Micro-manipulations par adhésion: Modélisations dynamiques et expérimentation, PhD thesis, Université Pierre et Marie Curie, Paris (2000).
25. A. McLachlan, Three-body dispersion forces, *Mol. Phys.* **7**, 423–427 (1964).
26. Y. Zhou and B. J. Nelson, Adhesion force modeling and measurement for micromanipulation, in: *Proc. of SPIE Microrobotics and Micromanipulation*, pp. 169–180 (1998).
27. M. Abramowitz and I. A. Stegun, *Handbook of Mathematical Functions with Formulas, Graphs, and Mathematical Tables*, Dover Publications, New York, NY (1965).
28. J. T. Feddema, P. Xavier and R. Brown, Micro-assembly planning with van der waals force, *Journal of Micromechatronics* **1** (2), 139–153 (2001).
29. A. Delandstheer, *Analyse II, Problèmes de Cauchy Pour EDO: Analyse Numérique*. Presses Universitaires de Bruxelles, Brussels (2001).
30. F. Arai, D. Ando, T. Fukuda, Y. Nonoda and T. Oota, Micro manipulation based on micro physics-strategy based on attractive force reduction and stress measurement, in: *Proc. of the IEEE/RSJ Intelligent Robots System*, pp. 236–241 (1995).
31. B. Vögeli and H. von Känel, AFM-study of sticking effects for microparts handling, *Wear* **238**, 20–24 (2000).
32. P. Lambert and A. Delchambre, Forces acting on microparts: towards a numerical approach for gripper design and manipulation strategies in micro-assembly, in: *Proc. of the 1st Int. Precision Assembly Seminar (IPAS)*, S. Ratchev and A. Delchambre (Eds), pp. 79–84. Bad Hofgastein (2003).
33. K. D. Papadopoulos and C.-C. Kuo, *Colloids Surf.* **46**, 115 (1990).
34. A. K. Segupta and K. D. Papadopoulos, *J. Colloid Interface Sci.* **152**, 534 (1992).
35. M. C. Herman and K. D. Papadopoulos, *J. Colloid Interface Sci.* **136**, 285 (1990).
36. M. C. Herman and K. D. Papadopoulos, *J. Colloid Interface Sci.* **142**, 331 (1991).
37. M. van den Tempel, *Adv. Colloid Interface Sci.* **3**, 137 (1972).
38. J. Lowell and A. C. Rose-Innes, Contact electrification, *Adv. Phys.* **29**, 947–1023 (1980).

39. Y. Rollot, S. Regnier and J.-C. Guinot, Simulation of micro-manipulations: Adhesion forces and specific dynamic models, *International Journal of Adhesion and Adhesives* **19**, 35–48 (1999).
40. L. Lee, Dual mechanism for metal-polymer contact electrification, *Journal of Electrostatics* **32**, 1–29 (1994).
41. W. R. Harper, *Contact and Frictional Electrification*. Clarenton Press, Oxford (1967).
42. W. R. Harper, The volta effect as a cause of static electrification, *Proceedings of the Royal Society of London, A* **205**, 83–103 (1951).
43. J. Lowell and A. Akande, Contact electrification of metals, *Journal of Physics D: Applied Physics* **8**, 53–63 (1975).
44. G. Castle and L. Schein, General model of sphere-sphere insulator contact electrification, *Journal of Electrostatics* **36**, 165–173 (1995).
45. C. Schonenberger, Charge flow during metal-insulator contact, *Journal of Physical Review* **45** (7), 3861–3864 (1992).
46. K. Hirabayashi, Dielectric theory of the barrier height at metal-semiconductor and metal-insulator interfaces, *Journal of Physical Review* **3** (12), 4023–4025 (1971).
47. A. Marmur, Tip-surface capillary interactions, *Langmuir* **9**, 1922–1926 (1993).
48. T. Stifter, O. Marti and B. Bhushan, Theoretical investigation of the distance dependence of capillary and van der Waals forces in scanning force microscopy, *Phys. Rev. B* **62** (20), 13667–13673 (2000).
49. W. M. van Spengen, MEMS reliability: stiction, charging and RF MEMS, PhD thesis, Katholieke Universiteit Leuven, Leuven (2004).
50. L. Zitzler, S. Herminghaus and F. Mugele, Capillary forces in tapping mode atomic force microscopy, *Phys. Rev. B* **66** (15), 155436 (2002).
51. O. Pitois and X. Chateau, Small particle at a fluid interface: Effect of contact angle hysteresis on force and work of detachment, *Langmuir* **18** (25), 9751–9756 (2002).
52. A. de Lazzer, M. Dreyer and H. J. Rath, Particle-surface capillary forces, *Langmuir* **15**, 4551–4559 (1999).
53. H. Grutzeck and L. Kiesewetter, Downscaling of grippers for micro assembly, *Microsystem Technologies* **8**, 27–31 (2002).
54. X. Pepin, D. Rossetti, S. M. Iveson and S. J. R. Simons, Modeling the evolution and rupture of pendular liquid bridges in the presence of large wetting hysteresis, *J. Colloid Interface Sci.* **232**, 289–297 (2000).
55. P. Lambert, P. Letier and A. Delchambre, Capillary and surface tension forces in the manipulation of small parts, in: *Proc. of Int. Symposium on Assembly and Tasks Planning (ISATP)*, pp. 54–59 (2003).
56. H. Grutzeck and L. Kiesewetter, Downscaling of grippers for micro assembly, in: *Micro System Technologies, Proc. of 6th Int. Conf. on Micro Electro, Opto Mechanical Systems and Components*, Potsdam (1998).
57. H. Grutzeck, Fluidisches Greifen in der Mikrosystemtechnik, PhD thesis, TU Cottbus, Cottbus (1999).
58. K. Johnson, *Contact Mechanics*, C.U.P. Edition (1985).
59. H. M. Pollock, What part does interfacial energy play in the deformation and adhesion of metals? *Vacuum* **31** (10-12), 609–617 (1981).
60. R. G. Horn, J. N. Israelachvili and F. Pribac, Measurement of the deformation and adhesion of solids in contact, *Journal of Colloid and Interface Science* **115** (2), 480–492 (1987).
61. K. L. Johnson, K. Kendall and A. D. Roberts, Surface energy and the contact of elastic solids, *Proc. R. Soc. Lond. A* **324**, 301–313 (1971).
62. B. V. Derjaguin, V. M. Muller and Yu. P. Toporov, Effect of contact deformations on the adhesion of particles, *Journal of Colloid and Interface Science* **53**, 314–326 (1975).
63. D. Maugis, Adhesion of spheres: the JKR-DMT transition model using a dugdale model, *Journal of Colloid and Interface Science* **150**, 243–269 (1992).

64. O. Pietrement, *Imagerie et caractérisation nanomécanique des surfaces par microscopie à force atomique*, PhD thesis, Université de Reims Champagne-Ardennes, Reims (2000).
65. R. W. Carpick, D. F. Ogletree and M. Salmeron, A general equation for fitting contact area and friction vs load measurements, *Journal of Colloid and Interface Science* **211**, 395–400 (1999).
66. D. Tabor, Friction — the present state of our understanding, *Journal of Lubrification Technology* **103**, 169–179 (1981).
67. Y. Ando and J. Ino, The effect of asperity array geometry on friction and pull-off force, *Journal of Tribology* **119**, 1–7 (1997).
68. J. Skinner and N. Gane, Sliding friction under a negative load, *Journal of Physics D: Applied Physics* **5**, 2087–2094 (1972).
69. D. S. Haliyo and S. Régnier, Manipulation of micro-objects using adhesion forces and dynamical effects, in: *Proceedings of ICRA/IEEE International Conference on Robotics and Automation*, (2002).
70. D. S. Haliyo, Y. Rollot and S. Régnier, Dynamical effects on releasing sticking objects manipulated by adhesion, in: *Proceedings of SPIE on Microrobotics and Microassembly* (2002).